

A NEW CONSTRAINT ON THE PHYSICAL NATURE OF DAMPED LYMAN ALPHA SYSTEMS

J. COOKE¹ & J.M. O'MEARA²
Draft version September 8, 2018

ABSTRACT

The formation and evolution of galaxies require large reservoirs of cold, neutral gas. The damped Lyman- α systems (DLAs), seen in absorption toward distant quasars and gamma-ray bursts, are predicted to be the dominant reservoirs for this gas. Detailed properties of DLAs have been studied extensively for decades with great success. However, their size, fundamental in understanding their nature, has remained elusive, as quasar and gamma-ray-burst sightlines only probe comparatively tiny areas of the foreground DLAs. Here, we introduce a new approach to measure the full extent of DLAs in the sightlines toward *extended* background sources. We present the discovery of a high-column-density ($\log N(\text{HI}) = 21.1 \pm 0.4 \text{ cm}^{-2}$) DLA at $z \sim 2.4$ covering 90–100% of the luminous extent of a line-of-sight background galaxy. Estimates of the size of the background galaxy range from a minimum of a few kpc^2 , to $\sim 100 \text{ kpc}^2$, and demonstrate that high-column density neutral gas can span continuous areas 10^8 – 10^{10} times larger than previously explored in quasar or gamma-ray burst sightlines. The DLA presented here is the first from a sample of DLAs in our pilot survey that searches Lyman break and Lyman continuum galaxies at high redshift. The low luminosities, large sizes, and mass contents ($\gtrsim 10^6$ – $10^9 M_\odot$) implied by this DLA and the early data suggest that DLAs contain the necessary fuel for galaxies, with many systems consistent with relatively massive, low-luminosity primeval galaxies.

Subject headings: galaxies: evolution — galaxies: high redshift — intergalactic medium — quasars: absorption lines

1. INTRODUCTION

Damped Ly α absorption systems (DLAs) contain the bulk of the neutral hydrogen (HI) in the Universe and play a dominant role in cosmic star formation (Wolfe et al. 2005; Wolfire et al. 2003). High-resolution spectra of DLAs in bright quasar and gamma-ray burst sightlines yield a wealth of information, such as their chemical composition, ionization states, and gas kinematics (e.g., Prochaska et al. 2007). However, these background sources probe areas of $< 0.01 \text{ parsec}^2$ at the DLA redshift and, as a result, the size of DLAs has remained elusive for ~ 40 years. Only by their spatial correlation with a known galaxy population has the average mass of DLAs been constrained (Gawiser et al. 2001; Adelberger et al. 2003; Bouché & Lowenthal 2004; Cooke et al. 2006). The situation improves dramatically when the background light source has a large spatial extent, such as a galaxy. Extended background sources can distinguish between DLAs that have large or small spatial extents via differences in their observed absorption-line depths and profiles, reflecting their covering fractions and column densities, respectively. In this Letter, we present the detection of a high-redshift DLA as the first result of a new program to determine DLA spatial extents as a population by searching comparatively high signal-to-noise ratio (S/N), low-resolution $z \gtrsim 2$ galaxy spectra. We assume an $H = 70$, $\Omega_M = 0.3$, $\Omega_\Lambda = 0.7$ cosmology throughout this paper, and all magnitudes are in the AB system (Fukugita et al. 1996).

2. DATA

Our program utilizes the publicly available VLT Vimos Deep Survey (VVDS) UltraDeep³ (Le Fèvre et al. 2003, 2013) using the 8.2m Very Large Telescope. To date, we searched for DLAs in 54 $z \sim 2$ –4 galaxy spectra that meet Lyman continuum galaxy (LCG; Cooke et al. 2014) criteria. The VVDS-UltraDeep consists of deep, ~ 18 hr spectroscopic integrations (~ 1200 s per exposure) that result in S/N ~ 5 –20 in the Ly α forest region of the galaxy spectra to search for absorption-line systems. VVDS-UltraDeep provides a bluer wavelength coverage (~ 3650 – 9350 \AA) as compared to the parent VVDS survey necessary for $z \sim 2$ –4 DLA searches. In addition, we searched for DLAs in 260 $z \sim 2$ –4 Lyman break galaxy (LBG; Steidel et al. 1995) spectra using LRIS (Oke et al. 1995; Steidel et al. 2004) and DEIMOS (Faber et al. 2003) on the 10m Keck telescopes between 2001 March to 2014 June as primary or secondary science for several programs (hereafter the Keck programs). Details of the observations and the color selection criteria are outlined in previous work (Cooke et al. 2005, 2013).

The Keck programs color select $R_{AB} \leq 25.5$ (or $i_{AB} \leq 25.5$) galaxies following the standard Lyman break technique that assumes little to no escaping Lyman continuum ($< 912 \text{ \AA}$) flux. Galaxies that produce Lyman continuum flux have observed colors inconsistent with Lyman break expectations with respect to their redshifts, but are found within, and outside of, the standard color selection criteria (Cooke et al. 2014). As a result, the Keck programs are only sensitive to galaxies with foreground DLAs having a combined color that remains within the standard LBG selection criteria. In contrast, VVDS-

¹ Centre for Astrophysics and Supercomputing, Swinburne University of Technology, Hawthorn, Vic 3122, Australia

² Department of Physics, Saint Michael's College, One Winooski Park, Colchester, VT 05439, USA

³ cesam.lam.fr/vvds/vvds_download.php

UltraDeep selects $i_{AB} > 24.75$ galaxies solely based on their magnitude (i.e., no color selection). We focus on the VVDS-UltraDeep spectra that exhibit excess u -band flux (LCGs), with most galaxies having colors outside of the standard LBG color selection criteria. These spectra are more likely to include lower-redshift line-of-sight systems with detectable emission as compared to LBGs.

We use the five-year stacked images ($m_{lim} \sim 27$) of the Canada-France-Hawaii Telescope Legacy Survey (CFHTLS) Deep Fields high-quality $u^*g'r'i'$ images⁴ (seeing FWHM $< 0.75''$) for photometric and morphological analysis. The imaging and spectroscopic data were reduced using standard IRAF and IDL procedures and the reduction pipelines of the facilities providing the data.

3. VVDS 910298177

Figure 1 presents the 1D and 2D spectra of the $z \sim 2.8$ galaxy VVDS 910298177 from the VVDS-UltraDeep survey. The spectral profile is typical of $z \sim 3$ LBGs with Ly α in emission. As seen in Figure 1, the spectra show a strong absorption feature near $\lambda \sim 4124\text{\AA}$. We interpret the feature as H I Ly α absorption. Visual inspection of the broad width of the absorption feature, which we refer to as EG1 for convenience, places it in the DLA regime.

Figure 2 presents $5'' \times 5''$ CFHTLS image cutouts centered on VVDS 910298177, with its properties listed in Table 1. The contours in Figure 2 suggest a non-point-source, asymmetric morphology that may be the result of either the extended morphology of the background galaxy or a blending of two sources corresponding to the background galaxy and emission from the DLA. In the latter case, the consistency of the image contours suggest that the DLA may reside at a projected separation of $\sim 1''$ (~ 8 physical kpc) to the southeast of the flux contour peaks.

3.1. The $z \sim 2.4$ DLA in the spectrum of VVDS 910298177

We first estimate the H I content of EG1 by measuring its equivalent width. The feature is centered near $\lambda = 4124 \text{\AA}$ ($z_{abs} = 2.391$), and we choose a conservative wavelength window 2500 km s^{-1} on either side ($4088.1\text{--}4156.9 \text{\AA}$) so as to avoid contaminating absorption (specifically, the feature near $\lambda \sim 4055 \text{\AA}$). These parameters result in a Ly α rest equivalent width $W_r \sim 17.0 \text{\AA}$ and a column density of $\log N(\text{H I}) \sim 20.8 \text{ cm}^{-2}$. We stress that this value underestimates the H I content as the damping wings have been neglected.

Next, we use a Voigt profile model centered at $z_{abs} = 2.391$ and adopt the flux level of the composite spectrum as an estimate of the continuum level. We find that the feature is well modeled at $\log N(\text{H I}) \sim 21.1 \text{ cm}^{-2}$. Uncertainties resulting from the S/N, low resolution, contaminating flux and absorption, and continuum level allow for a range of model fits. Thus, we conservatively adopt an H I content estimate of $\log N(\text{H I}) = 21.1 \pm 0.4$ as illustrated in Figure 1.

We stress that the models and our simulations of the feature *require* that EG1 have this H I column density

covering $\gtrsim 90\%$ of the background galaxy (i.e., a covering factor, $f_c \gtrsim 0.9$). If EG1 had an equivalent H I column density but only covered a small region of the background galaxy, the damping wings would not be as pronounced and the core region would deviate significantly from zero (i.e., much shallower than observed) because of the low resolution of the VVDS-UltraDeep spectrum (Schaye 2001; Heckman et al. 2001).

4. THE PHYSICAL NATURE OF EG1

The size of VVDS 910298177 cannot be determined accurately using seeing-limited ground-based data. However, we can place meaningful constraints on its size as follows. The most physically compact morphology to produce the star-forming luminosity of VVDS 910298177 ($M \sim -21$) would be that of a highly dense ~ 1 kpc super-star-forming clump. Such a compact background galaxy would probe continuous areas of the DLAs $\gtrsim 100,000,000$ larger than that probed by quasars and gamma-ray-burst sightlines. Galaxies at $z \sim 2\text{--}3$ with luminosities similar to, and fainter than, VVDS 910298177 have average half-light radii of $1\text{--}3$ kpc and a variety of morphologies – from single compact star-forming regions to extended diffuse emission with multiple star-forming clumps – and include systems with radii of ~ 10 kpc to the surface brightness limits of the deep VVDS-UltraDeep spectroscopy (Förster Schreiber et al. 2009; Elmegreen & Elmegreen 2005; Law et al. 2012b,a). If VVDS 910298177 is typical of $z \sim 3$ galaxies, the continuous area of EG1 probed would range from a few to $\sim 100 \text{ kpc}^2$. Previous research using the radio structure of quasars, radio mapping, infrared adaptive optics observations, and quasar close pair sightlines (Briggs et al. 1989; Zwaan et al. 2005; Ellison et al. 2007; Monier et al. 2009; Cooke et al. 2010; Krogager et al. 2012; Jorgenson & Wolfe 2014) suggests that DLAs span these extents.

Under the simple assumption that the DLA gas resides in a uniform slab, the range of background galaxy sizes ($1\text{--}100 \text{ kpc}^2$) and 1σ column densities correspond to neutral gas masses of $\sim 10^6\text{--}10^9 M_\odot$ using $(\text{H I}(\text{cm}^{-2}) \times A(\text{cm}^2) \times m_{\text{proton}}(g))/1.98 \times 10^{33} \text{ g}/M_\odot$.

The mass estimate only considers the area probed by the background galaxy flux and, because gas densities in DLA clouds should diminish toward their outer radii, a significant fraction of the gas may extend over larger areas. The mass estimate is consistent with DLA gas associated with $z \sim 3$ DLA dark matter halos from observation (Cooke et al. 2006) and theory (e.g., Fumagalli et al. 2011; Rahmati & Schaye 2014).

Such large reservoirs of self-shielded neutral gas are protogalaxies, or extended components of established galaxies, and are expected to produce significant star formation as the system evolves. Inspection of the images reveals a subtle elongation in the shape of VVDS 910298177 and, interestingly, faint flux may be present in the 2D spectrum offset from the Ly α absorption (below the spectrum as shown in Figure 1) and spatially consistent with the elongation. If real, these features may result from emission by EG1 and imply that it is a faint galaxy.

To test this hypothesis, we conservatively assume that the background galaxy produces zero Lyman continuum flux (which, here, falls in the u^* -band) following the Lyman break expectations (Steidel & Hamilton 1993; Stei-

⁴ www.cfht.hawaii.edu/Science/CFHLS/

del et al. 2003). We note that some $z \sim 3$ galaxies are theorized, and observed, to exhibit Lyman continuum flux of a few percent as compared to their flux near 1500\AA (Steidel et al. 2001; Cooke et al. 2014). A photometric and spectroscopic comparison of VVDS 910298177 finds that the slit spectroscopy acquired $\sim 52\%$ of the total galaxy flux in the $g'r'i'$ filters. We apply this correction to the u^* -band and conservatively assign all excess u^* -band flux of the background galaxy to the DLA. This approach yields a DLA brightness of $m(1000\text{\AA}) \sim 27.1$, corresponding to roughly $m(1500\text{\AA}) = 26.3$, a star formation rate of $\sim 2 M_{\odot} \text{ yr}^{-1}$, and a halo mass $M_{DM} \sim 10^{11} M_{\odot}$ (Berrier & Cooke 2012). These upper limits are consistent with the offset flux observed in the images, the values found in DLA emission searches in quasar sightlines (Møller et al. 2002; Fynbo et al. 2011; Péroux et al. 2012; Krogager et al. 2012; Jorgenson & Wolfe 2014; Fumagalli et al. 2015), and the number density of $m_i \sim 27$ $z \sim 3$ galaxies (Schaye 2001). The above test demonstrates that an interpretation of EG1 as a high-redshift galaxy is plausible (see also §6).

5. THE OCCURRENCE RATE OF DLAS IN GALAXY SPECTRA

As a first step to estimate the occurrence rate of DLAs in galaxy spectra, we assess the frequency of absorbers having similar HI column densities as EG1 in quasar spectra. The VVDS 910298177 spectrum provides a redshift path $z = 1.96\text{--}2.81$ to search for DLA Ly α absorption, corresponding to a cosmological pathlength of $\Delta X = 2.768$. The DLA incidence frequency is $\ell(X)$, where the number of DLAs in pathlength ΔX is given by $\ell(X)\Delta X$. If we adopt the $z \sim 2.5$ HI column density distribution function of Noterdaeme et al. (2012), we find $\ell(X) = 0.025$ for DLAs in the allowed $N(\text{HI})$ range of EG1 ($\log N(\text{HI}) = 21.1 \pm 0.4 \text{ cm}^{-2}$). Thus, we would have to observe ~ 14 quasars probing redshift range $z = 1.96\text{--}2.81$ to detect one DLA with the same HI content. If we restrict ourselves to the range $\log N(\text{HI}) 21.1 \pm 0.05 \text{ cm}^{-2}$, the number of quasars needed increases to ~ 150 , owing to the steep shape of the HI column density distribution function. Thus, while uncommon, absorbers like EG1 are not exceedingly rare when observed in quasar spectra. Current simulations indicate that absorbers with sizes and column densities similar to EG1 comprise $\sim 1\%$ of the DLA population (Fumagalli et al. 2011; Rahmati & Schaye 2014).

While the full analysis for our program sample will appear in later papers, we can make initial estimates of the incidence frequency of DLAs in galaxy sightlines. From the 54 secure VVDS-UltraDeep LCG spectra that we assessed, we find two additional DLA candidate systems ($W_r(\text{Ly}\alpha) > 5\text{\AA}$), providing a coarse $\sim 6\%$ occurrence rate estimate for systems with $\log N(\text{HI}) \gtrsim 20.3 \text{ cm}^{-2}$ and $\sim 2\%$ for systems with $\log N(\text{HI}) \gtrsim 21.1 \text{ cm}^{-2}$. Depending on significance level, we find ~ 6 DLA candidate systems in the lower S/N Keck programs LBG spectra. Under the assumption that these ~ 6 systems are DLAs, their occurrence rates are $\sim 3\text{--}5\times$ lower than the VVDS-UltraDeep LCGs.

As described in §4, excess Lyman continuum flux in LCGs with DLAs could result from DLA galaxy emission. If the difference in the estimated LCG and LBG

occurrence rates persists with larger statistical samples, the results would support the scenario in which DLAs often produce detectable flux and, thus, are associated with star-forming galaxies (Møller et al. 2002; Cooke et al. 2006; Fynbo et al. 2011; Péroux et al. 2012; Krogager et al. 2012; Jorgenson & Wolfe 2014). DLAs in galaxy sightlines provide opportunities to measure their host galaxy properties without the glare typically present from bright quasars.

6. GALAXIES WITH DOMINANT Ly α IN ABSORPTION AND THE NATURE OF THE NEUTRAL GAS

Previous work analysing $r \lesssim 25.5$ LBG spectra (e.g., Shapley et al. 2003; Cooke et al. 2006) find that roughly 25% exhibit dominant Ly α in absorption, $\sim 25\%$ show dominant Ly α in emission, and the remainder exhibit a combination of Ly α emission and absorption. Many LBGs with dominant Ly α absorption show evidence for damped absorption (Pettini et al. 2000; Shapley et al. 2003). Finally, a population of faint, high-redshift Ly α emitting galaxies (LAEs) have been identified via the detection of Ly α emission in narrowband imaging surveys (e.g., Hu et al. 1998) and appear to be similar to the $\sim 25\%$ of LBGs that show Ly α in emission but have bluer UV continuum slopes and lower star formation rates (Gawiser et al. 2006; Cooke 2009; Cooke et al. 2013; Garel et al. 2015).

Spectra of faint ($r \gtrsim 25.5$) LBGs with an S/N of more than a few are difficult to obtain with 8 m class telescope in reasonable integration times. The spectra acquired to date show a trend for a larger fraction of galaxies showing Ly α in emission. This trend may be an observational bias because very faint galaxy spectra are easier to identify when Ly α emission is present. As a result, the identification of $r \gtrsim 25$ galaxies with dominant Ly α in absorption (LAAs) and their properties remain largely unknown. DLAs randomly sample all galaxies with sufficient neutral gas, including very faint and low-mass galaxies. Here, we examine the likelihood that EG1 is an LAA.

To model the VVDS 910298177 spectrum as two galaxies, we first use a composite spectrum constructed from ~ 200 $r < 25.5$ LBG spectra with dominant Ly α in emission to model the background galaxy (hereafter eLBG spectrum). To model EG1, we use a composite spectrum constructed from ~ 200 $r < 25.5$ LBGs with dominant Ly α in absorption (hereafter aLBG spectrum). We place the eLBG spectrum at the redshift of the background galaxy and scale it to the 1500\AA flux of the background galaxy minus the upper limit flux of EG1 ($r' = 26.3$). We then overlay and scale the aLBG spectrum to the redshift and 1500\AA flux of EG1. Finally, we note that EG1 is in the foreground and its damped Ly α absorption feature will absorb the background galaxy flux (i.e., not be convolved with it). We scale the template to reflect a $\sim 90\%$ absorption to match the lower limit of the data. Figure 3 shows the resulting composite spectrum (eLBG+aLBG) overlaid onto the data.

The Ly α feature of the aLBG spectrum is in very good agreement with the Ly α feature of EG1 in profile, depth, and width (i.e., EG1 is similar to an LAA) when considered in the proper context. The Ly α absorption in the composite aLBG spectrum results largely from absorption foreground to star-forming regions in the LBGs

that compose it. In contrast, all the gas in EG1 absorbs the background galaxy, including advancing and receding gas as a result of outflows. The red portion of the aLBG spectrum Ly α feature does not include absorption from receding gas nor the circumgalactic material on the far side of EG1 and includes Ly α flux from resonantly scattered photons of the LBGs with higher star formation rates that compose it.

Interestingly, VVDS 910298177 exhibits a strong absorption feature blueward of EG1 Ly α similar to the Si II 1193 Å, Si III 1200, 1207 Å feature in the aLBG spectrum, and there is low S/N evidence for Si II 1260, 1304, 1527 Å and Si IV 1393, 1403 Å absorption by EG1. If real, this behavior implies a large Si covering fraction for EG1 and similar properties to $r \lesssim 25.5$ LAAs.

Finally, we test the assumption that DLAs are galaxies like LBGs using their number density. Previous work shows that the number density of DLAs and $z \sim 3$ $r \lesssim 27$ LBGs (i.e., $n = 0.016 h^3 \text{Mpc}^{-3}$; $M_{DM} \gtrsim 10^{11} M_{\odot}$) are consistent if DLAs have average radii of 19 kpc (Schaye 2001). However, most DLAs are likely fainter than $r \lesssim 27$, as our sample and unbiased searches indicate (Fumagalli et al. 2015).

If, instead, we assume DLAs have average radii of ~ 5.7 kpc (i.e., average areas of 100 kpc²), they would sample $r' \lesssim 30$ LBGs ($M \sim -15.5$; $M_{DM} \gtrsim 10^{10.7} M_{\odot}$) with an extrapolation of the LBG luminosity function (e.g., Reddy & Steidel 2009). This speculation is plausible, given the estimated areas of DLAs in our sample and because $\log N(\text{HI}) > 20.3$ gas likely extends to areas larger than that probed by the background galaxies.

Finally, we note that UV-luminous LBGs do not comprise all galaxies at high redshift, and there is evidence that they may constitute as little as ~ 15 – 20% (Berrier & Cooke 2012; Spitler et al. 2014). Because DLAs randomly probe galaxies independent of their UV luminosities, average radii of ~ 5.7 kpc would probe $r \lesssim 28$ galaxies at $z \sim 3$ in such a scenario, allowing much smaller average DLA radii when probing average galaxies by number.

7. THE FUTURE

The discovery of high-redshift DLAs in sightlines to galaxies provides the first means to uncover their true sizes. Our approach of searching LBG and LCG sightlines exploits commonly occurring galaxies, as opposed to rare quasars and gamma ray bursts, while probing continuous areas more than 10 million times larger. Future analysis of our full DLA sample will include background galaxy sizes determined from Cycle 23 *Hubble Space Telescope* imaging (GO 14160; PI: O’Meara).

The general approach pushes the capabilities of 8 m class telescope facilities to their limits. However, searches for DLAs in the sightlines to background galaxies will likely become the dominant method of study in the upcoming era of 30 m class telescopes. Nominal first light instruments enable $R = 5000$ spectroscopy of $m < 24.5$ galaxies at $S/N > 35$ in 4.5 hr (e.g., WFOS on the Thirty Meter Telescope). The increase in both resolution and S/N would enable more accurate $N(\text{HI})$ and metallicity measurements. In addition, lower-resolution spectroscopy ($R \sim 1000$), enables $>5\sigma$ DLA detection in $m < 26.5$ galaxy spectra in 1 hr.

Probing to fainter galaxies dramatically increases the number density, enabling a tomographic neutral gas mass reconstruction of the early Universe, while helping to complete our understanding of galaxy formation and evolution.

JC thanks Olivier Le Fèvre and Michael Murphy for helpful discussions. JC acknowledges support from Australian Research Council grant FF130101219. JMO thanks the Swinburne Visiting Scientist scheme that helped make this work possible. This research uses data from the VIMOS VLT Deep Survey, obtained from the VVDS database operated by Cesam, Laboratoire d’Astrophysique de Marseille, France. In addition, some of the data presented here are based on observations obtained with MegaPrime/MegaCam, a joint project of CFHT and CEA/IRFU, at the Canada-France-Hawaii Telescope (CFHT) which is operated by the National Research Council (NRC) of Canada, the Institut National des Science de l’Univers of the Centre National de la Recherche Scientifique (CNRS) of France, and the University of Hawaii. This work is based in part on data products produced at Terapix available at the Canadian Astronomy Data Centre as part of the Canada-France-Hawaii Telescope Legacy Survey, a collaborative project of NRC and CNRS. Finally, some of the data presented herein were obtained at the W.M. Keck Observatory, which is operated as a scientific partnership among the California Institute of Technology, the University of California and the National Aeronautics and Space Administration. The Observatory was made possible by the generous financial support of the W.M. Keck Foundation. The authors wish to recognize and acknowledge the very significant cultural role and reverence that the summit of Mauna Kea has always had within the indigenous Hawaiian community. We are most fortunate to have the opportunity to conduct observations from this mountain.

REFERENCES

- Adelberger, K. L., Steidel, C. C., Shapley, A. E., & Pettini, M. 2003, *ApJ*, 584, 45
- Berrier, J. C., & Cooke, J. 2012, *MNRAS*, 426, 1647
- Bouché, N., & Lowenthal, J. D. 2004, *ApJ*, 609, 513
- Briggs, F. H., Wolfe, A. M., Liszt, H. S., Davis, M. M., & Turner, K. L. 1989, *ApJ*, 341, 650
- Cooke, J., Wolfe, A. M., Prochaska, J. X., & Gawiser, E. 2005, *ApJ*, 621, 596
- Cooke, J., Wolfe, A. M., Gawiser, E., & Prochaska, J. X. 2006, *ApJ*, 652, 994
- Cooke, J. 2009, *ApJ*, 704, L62
- Cooke, J., Omori, Y., & Ryan-Weber, E. V. 2013, *MNRAS*, 433, 2122
- Cooke, J., Ryan-Weber, E. V., Garel, T., & Díaz, C. G. 2014, *MNRAS*, 441, 837
- Cooke, R., Pettini, M., Steidel, C. C., King, L. J., Rudie, G. C., & Rakić, O. 2010, *MNRAS*, 409, 679
- Ellison, S. L., Hennawi, J. F., Martin, C. L., & Sommer-Larsen, J. 2007, *MNRAS*, 378, 801
- Elmegreen, B. G., & Elmegreen, D. M. 2005, *ApJ*, 627, 632
- Faber, S. M., et al. 2003, in *Society of Photo-Optical Instrumentation Engineers (SPIE) Conference Series*, Vol. 4841, *Instrument Design and Performance for Optical/Infrared Ground-based Telescopes*, ed. M. Iye & A. F. M. Moorwood, 1657–1669
- Förster Schreiber, N. M., et al. 2009, *ApJ*, 706, 1364
- Fukugita, M., Ichikawa, T., Gunn, J. E., Doi, M., Shimasaku, K., & Schneider, D. P. 1996, *AJ*, 111, 1748

- Fumagalli, M., Prochaska, J. X., Kasen, D., Dekel, A., Ceverino, D., & Primack, J. R. 2011, *MNRAS*, 418, 1796
- Fumagalli, M., O’Meara, J. M., Prochaska, J. X., Rafelski, M., & Kanekar, N. 2015, *MNRAS*, 446, 3178
- Fynbo, J. P. U., et al. 2011, *MNRAS*, 413, 2481
- Garel, T., Blaizot, J., Guiderdoni, B., Michel-Dansac, L., Hayes, M., & Verhamme, A. 2015, *MNRAS*, 450, 1279
- Gawiser, E., Wolfe, A. M., Prochaska, J. X., et al. 2001, *ApJ*, 562, 628
- Gawiser, E., et al. 2006, *ApJ*, 642, L13
- Heckman, T. M., Sembach, K. R., Meurer, G. R., Leitherer, C., Calzetti, D., & Martin, C. L. 2001, *ApJ*, 558, 56
- Hu, E. M., Cowie, L. L., & McMahon, R. G. 1998, *ApJ*, 502, L99
- Jorgenson, R. A., & Wolfe, A. M. 2014, *ApJ*, 785, 16
- Krogager, J.-K., Fynbo, J. P. U., Møller, P., Ledoux, C., Noterdaeme, P., Christensen, L., Milvang-Jensen, B., & Sparre, M. 2012, *MNRAS*, 424, L1
- Law, D. R., Steidel, C. C., Shapley, A. E., Nagy, S. R., Reddy, N. A., & Erb, D. K. 2012a, *ApJ*, 759, 29
- . 2012b, *ApJ*, 745, 85
- Le Fèvre, O., et al. 2003, in *Society of Photo-Optical Instrumentation Engineers (SPIE) Conference Series*, Vol. 4841, *Instrument Design and Performance for Optical/Infrared Ground-based Telescopes*, ed. M. Iye & A. F. M. Moorwood, 1670–1681
- Le Fèvre, O., et al. 2013, *A&A*, 559, A14
- Møller, P., Warren, S. J., Fall, S. M., Fynbo, J. U., & Jakobsen, P. 2002, *ApJ*, 574, 51
- Monier, E. M., Turnshek, D. A., & Rao, S. 2009, *MNRAS*, 397, 943
- Noterdaeme, P., et al. 2012, *A&A*, 547, L1
- Oke, J. B., Cohen, J. G., Carr, M., Cromer, J., Dingizian, A., Harris, F. H., Labrecque, S., Lucinio, R., Schaal, W., Epps, H., & Miller, J. 1995, *PASP*, 107, 375
- Péroux, C., Bouché, N., Kulkarni, V. P., York, D. G., & Vladilo, G. 2012, *MNRAS*, 419, 3060
- Pettini, M., Steidel, C. C., Adelberger, K. L., Dickinson, M., & Giavalisco, M. 2000, *ApJ*, 528, 96
- Prochaska, J. X., Chen, H.-W., Dessauges-Zavadsky, M., & Bloom, J. S. 2007, *ApJ*, 666, 267
- Rahmati, A., & Schaye, J. 2014, *MNRAS*, 438, 529
- Reddy, N. A., & Steidel, C. C. 2009, *ApJ*, 692, 778
- Schaye, J. 2001, *ApJ*, 559, L1
- Shapley, A. E., Steidel, C. C., Pettini, M., & Adelberger, K. L. 2003, *ApJ*, 588, 65
- Spitler, L. R., et al. 2014, *ApJ*, 787, L36
- Steidel, C. C., & Hamilton, D. 1993, *AJ*, 105, 2017
- Steidel, C. C., Pettini, M., & Hamilton, D. 1995, *AJ*, 110, 2519
- Steidel, C. C., Pettini, M., & Adelberger, K. L. 2001, *ApJ*, 546, 665
- Steidel, C. C., Adelberger, K. L., Shapley, A. E., Pettini, M., Dickinson, M., & Giavalisco, M. 2003, *ApJ*, 592, 728
- Steidel, C. C., Shapley, A. E., Pettini, M., Adelberger, K. L., Erb, D. K., Reddy, N. A., & Hunt, M. P. 2004, *ApJ*, 604, 534
- Wolfe, A. M., Gawiser, E., & Prochaska, J. X. 2005, *ARA&A*, 43, 861
- Wolfire, M. G., McKee, C. F., Hollenbach, D., & Tielens, A. G. G. M. 2003, *ApJ*, 587, 278
- Zwaan, M. A., van der Hulst, J. M., Briggs, F. H., Verheijen, M. A. W., & Ryan-Weber, E. V. 2005, *MNRAS*, 364, 1467

VVDS-UltraDeep Name	R.A. (J2000)	Decl. (J2000)	m_{u^*}	$m_{g'}$	$m_{r'}$	$m_{i'}$
	h m s	d m s	(AB)	(AB)	(AB)	(AB)
VVDS 910298177	02 26 54.699	-04 18 45.77	25.699 ± 0.091	24.751 ± 0.037	24.543 ± 0.035	24.535 ± 0.040

Table 1
Properties of VVDS 910298177

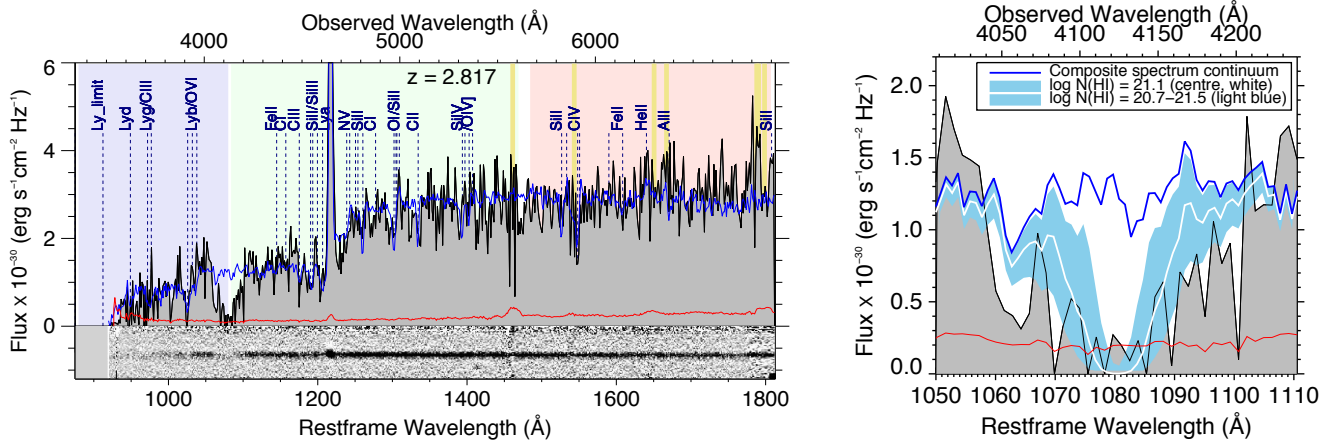


Figure 1. Spectra of the $z = 2.818$ galaxy VVDS 910298177. Left: the 1D spectrum (black) and 1σ error (red) are shown above zero flux, with the 2D spectrum inserted below zero flux for comparison. A composite $z \sim 3$ galaxy spectrum is overlaid (blue) with common atomic transitions labeled (dashed vertical lines) and the positions of bright night sky emission lines marked (thick yellow vertical lines). The DLA is seen near 1080\AA , restframe (4120\AA , observer-frame) and the $u^*g'r'$ CFHT Megacam filter bandpasses are indicated by the blue, green, and red shaded regions, respectively. Right: zoom-in of the spectrum centered on the DLA. A Voigt profile fit to the absorption (white curve) yields $\log N(\text{H I}) = 21.1 \pm 0.4$ atoms cm^{-2} (light blue shaded region).

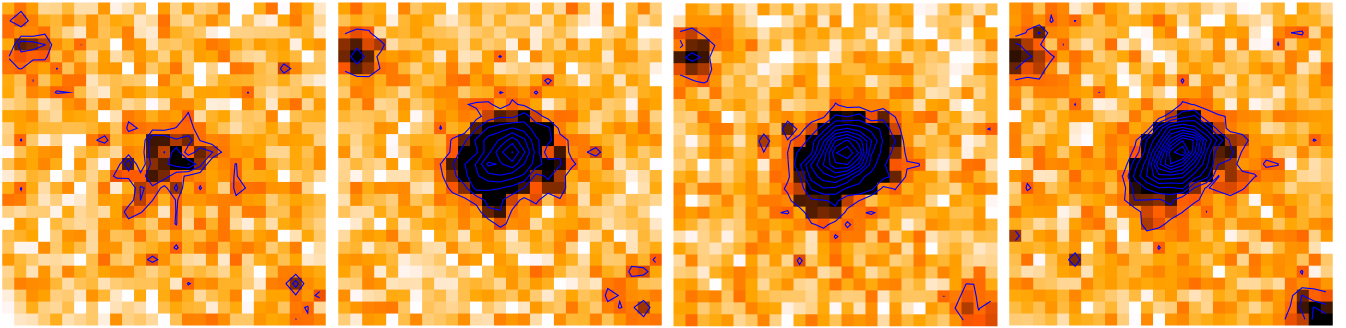


Figure 2. Thumbnail images of VVDS 910298177 (seeing $\text{FWHM} < 0.75''$) $5''$ on a side, or ~ 40 physical kpc at the background galaxy and DLA redshift. Left to right: the CFHTLS 5-year stacked u^* -, g' -, r' -, and i' -band images, respectively. Linearly increasing flux contours are overlaid in blue to help visualize the galaxy morphology. The first (outermost) contour corresponds to the 1σ sensitivity of the spectrum near the $\text{Ly}\alpha$ absorption feature.

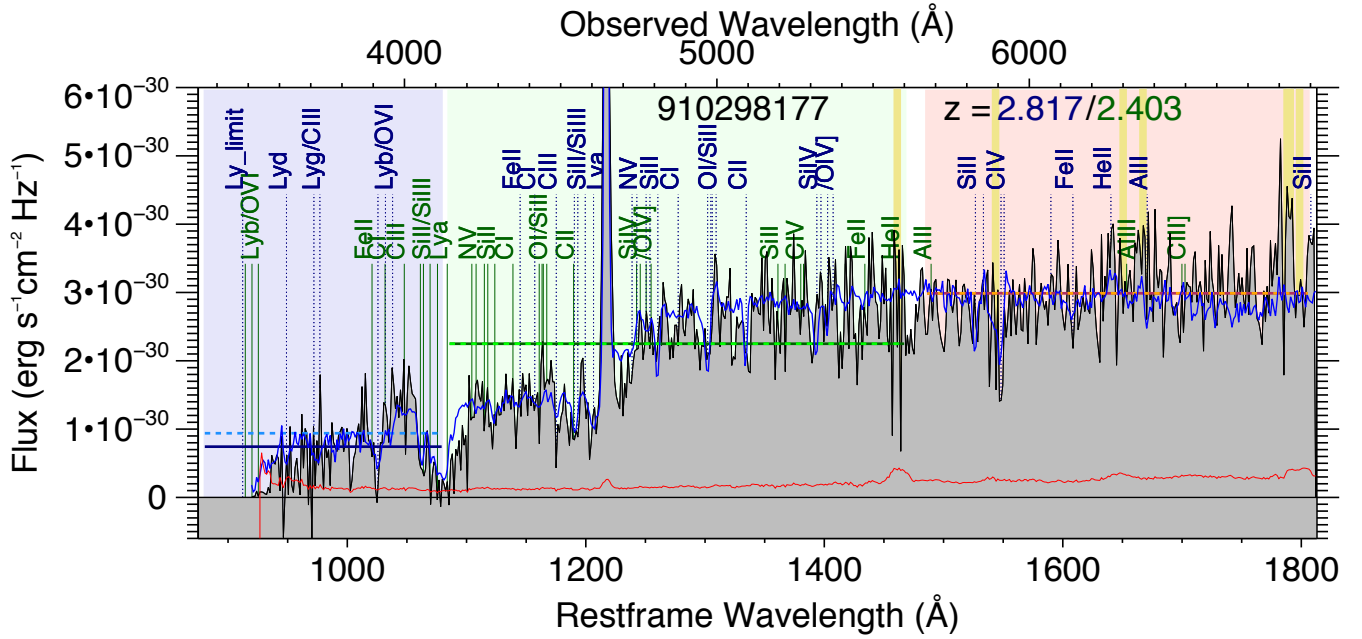


Figure 3. One-dimensional spectrum of EG1 and background galaxy plotted similarly to Figure 1. The composite spectrum (blue) is composed of ~ 200 $z \sim 3$ LBGs with dominant Ly α in emission (eLBG spectrum) at the redshift of the background galaxy ($z = 2.817$) and ~ 200 LBGs with dominant Ly α in absorption (aLBG spectrum) at the redshift of EG1 ($z = 2.403$). The eLBG spectrum is a good fit to the background galaxy, as shown in Figure 1, and the aLBG spectrum is added to model EG1. Prominent atomic transitions for the background galaxy (blue labels, upper row) and EG1 (green labels, lower row) are indicated. Solid horizontal lines represent the photometric flux levels for the u^* , g' , and r' filter bandpasses (blue, green, and red, respectively) using the r' -band correction factor (see the text). The dashed horizontal lines denote the mean spectrum flux over that bandpass.